A Four-Port Scattering Matrix Formalism for p-i-n Traveling-Wave Photodetectors

Isabelle Huynen, *Member, IEEE*, and André Vander Vorst, *Fellow, IEEE*

***Abstract*—This paper presents a full four-port characterization for traveling-wave optoelectronic devices, in particular, traveling-wave photodetectors (TWPD's), resulting in a scattering matrix formalism, which can be used for passive as well as active devices. A set of coupled distributed equivalent circuits is proposed for modeling the device, taking into account the wanted detection and spurious emission of light. A scattering matrix formalism is established, predicting the performances of the device at microwaves, when a microwave signal is used either for modulating the intensity of the optical power (forward detection mode) or for biasing the p-i-n junction (reverse emission mode). Hence, the obtained four-port device is nonreciprocal. Some symmetry properties are induced by the physical symmetry of the device. It has matched inputs, when symmetric electrical and optical reference loads are used. The scattering matrix satisfies power conservation laws. The formalism may be used to optimize the designs of TWPD's by varying the loads at each of the four ports.**

***Index Terms*—Photodetectors, p-i-n, scattering matrix, traveling wave.**

INTRODUCTION

AN OPTICAL communications system is basically composed of an electrooptical transducer (E/O), an optical transmission line, and an opto-electrical transducer (O/E). At the input, an electrical signal extending up to millimeter-wave frequencies modulates the intensity of the optical carrier. The output is demodulated by the O/E transducer, and the electrical signal is recovered.

This paper focuses on a specific O/E transducer, the p-i-n traveling-wave photodetector (TWPD) [1]–[4]. In TWPD's, the RF modulating envelope of the optical carrier and the RF photogenerated signal travel with the same velocity toward the accesses of the device. They are not reflected if those accesses are matched. Under such conditions, the bandwidth of TWPD's is limited only by microwave losses, which makes TWPD's superior to vertically illuminated and waveguide photodetectors.

E/O and O/E devices are characterized either by a large- or a small-signal analysis. The *large-signal* analysis considers the optical signal from the carrier point-of-view, summing up two vectors, for the optical carrier and modulation, respectively. For instance, an optical admittance matrix characterizes an all-dielectric asymmetrical multilayered structure [5], and a classical transformation yields the scattering matrix. However, this S-matrix is not adequate for characterizing E/O or O/E transducers. It indeed requires a linear relationship between the microwave and optical fields, which only exists between optical power and biasing electrical current, provided that the laser source operates in its linear range. This usually limits the analysis to electrical modulating signals of relatively small magnitude. The *small-signal* approach considers the optical signal from the modulation point-of-view only. It yields a vector linear relationship between the microwave signal and alternate component of the optical power, which is the modulated part of the power magnitude. Contributions have been published using this approach in time domain [6] and frequency domain [7]; however, without referring to an S-matrix formalism. Curtis and Ames [8] characterize a small-signal vector approach by an S-matrix; however, without considering the impedance level at the ports.

To obtain a full four-port characterization, we first developed an S-matrix definition [9] for transducers and optical components, which is fully compatible with the classical S matrix [10]. In this paper, we show that our S-matrix definition can be used for modeling TWPD's as four-, three-, or two-port. Adequate distributed RF and optical equivalent circuits describe the forward detection (O/E) and the reverse emission mode (E/O) of the p-i-n line, acting as a four-port coupler having both an electrical and optical port at each of its two physical accesses. Vector relationships are established between the optical or RF power quantities at each access. Using this formalism, several three- and two-port configurations are investigated. A power conservation relationship is derived for the four-port transducer. Throughout this paper, the subscripts E, O, and RF are used to designate electrical and optical quantities, and the modulation of the optical carrier, respectively, to avoid ambiguity.

I. TOPOLOGY

Fig. 1(a) and (b) shows two typical geometries of TWPD's, consisting of a multilayered transmission line, whose layers involve highly doped P^+ and N^+ zones, separated by an intrinsic zone. The p-i-n junction is reverse biased at dc so that the intrinsic area is fully depleted, with a zero equivalent conductivity. Microwave and optical propagation occur along the z-axis. The RF modulated part of the optical power intensity induces an RF variation of the photogenerated current in the intrinsic area,

Manuscript received March 17, 1999. This work was supported by the National Fund for Scientific Research, Belgium This work was supported in part by the Belgian Federal Office for Scientific, Technical, and Cultural Affairs under Contract PAI-IV/13.

The authors are with the Microwaves Department, Université Catholique de Louvain, B-1348 Louvain-la-Neuve, Belgium (e-mail: huynen@emic.ucl.ac.be).

Publisher Item Identifier S 0018-9480(00)04665-2.

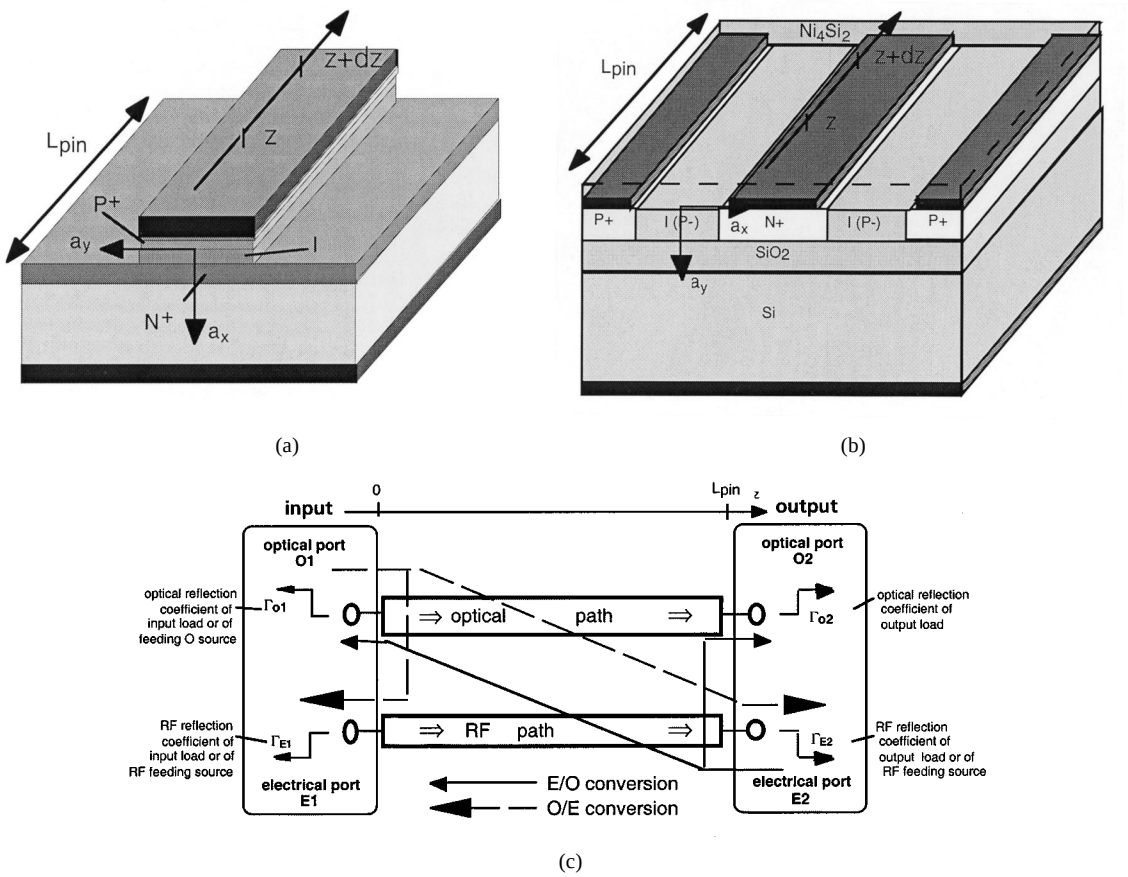

Fig. 1. Traveling-wave p-i-n phodetector topologies. (a) Mesa geometry. (b) Coplanar geometry. (c) Equivalent four-port configuration.

which is collected at the conductors and propagates along the equivalent RF transmission line.

II. Assumptions

The structures of Fig. 1(a) and (b) can be viewed as four-port couplers [see Fig. 1(c)]. At each physical access of the photodetector, noted respectively as input (1) and output (2), two ports are considered: electrical (E) and optical (O), respectively. At the electrical ports, i.e., $E1$ and $E2$, an RF signal is either applied as a source or collected from the distributed RF photogenerated current source. At the optical ports, i.e., $O1$ and $O2$, the baseband electrical RF signal modulating the optical power is either applied as a source or collected from the distributed laser effect. We consider indeed that a distributed laser emitting effect may occur when one of the accesses of the TPWD is fed by an RF signal. Hence, the modulated part of light emission can be collected at an optical port while only RF signals are feeding the structure.

As a consequence, the two following modes of operation are considered.

- *The (wanted) forward mode*: with a modulated optical beam incident at the input of the TWPD and no baseband electrical signals feeding its accesses. The modulated optical power applied at $O1$ is converted into an RF current during its propagation over the length of the device $L_{\rm pin}$, while the unconverted optical fraction flows into the equivalent load at $O2$, with an optical reflection coefficient Γ_{O2}. The distributed photogenerated RF current splits into two parts traveling in opposite directions. They are collected at $E1$ and $E2$, respectively, in loads having RF reflection coefficients Γ_{E1} and Γ_{E2}, respectively.
- *The (spurious) reverse mode*: with only an RF signal applied at $E2$, inducing the propagation of an RF signal biasing the distributed junction, which yields a progressive modulation of the light emitted over the length of the device. The fraction of optical power emitted at each abscissa of the length $L_{\rm pin}$ splits into two equal parts, traveling each toward one access. They are collected at $O1$ or $O2$, in loads having optical reflection coefficients Γ_{O1} and Γ_{O2}, respectively.

These forward and reverse modes characterize the four-port behavior once reference electrical and optical charges are defined at each access. We assume that the TWPD is symmetric with respect to the plane $z = L_{\rm pin}/2$. This physical symmetry induces some symmetry properties in the four-port scattering matrix. However, the matrix is not symmetrical because the forward detection and reverse emission modes are not reciprocal.

In practice, matched and open loads are considered. The structure reduces to a three-port when port $E1$ is open-ended while port $O2$ is optically matched. Moreover, when the output of the TWPD acts as an open load at optical wavelengths, the three-port coupler reduces to a classical two-port, either O/E or E/O.

The scattering matrix formalism derived in this paper is defined as "intrinsic," which means that the optical and RF feeders are "matched sources." From the RF point-of-view, reflections at any fed access are due only to reflections along the length of the structure or at another access. From the optical point-of-view, the word "intrinsic" means that the optical coupling efficiency is assumed equal to unity at each optical fed access: no power of the feeding light beam is reflected. As a consequence, the four-port S-matrix satisfies input matching conditions at all ports ($S_{ii} = 0$).

III. Equivalent Circuits for Forward Detection Mode

A. Transmission-Line Model for RF Power Modulating Optical Power

1) Power Scattering Waves: The optical power resulting from the modulation of an optical beam at frequency f_O by an RF signal at frequency $f_{\rm rf}$ is the sum of two optical beams P_1 and P_2, having same intensity and polarization, operating at frequencies f_O and $f_O + f_{\rm rf}$, respectively [11]. Noting $\bar{E}_1$ and $\bar{E}_2$, the electric fields corresponding to each optical signal, and $\bar{E}$, the total electric field, yields

$$\begin{aligned}\overline{E_O}(x,y,z) &= \bar{E}_1(x,y,z) + \bar{E}_2(x,y,z)\\ &= \bar{E}_O(x,y)e^{j\omega_O t}e^{-j\beta(\omega_O)z}e^{-\alpha(\omega_O)z}\\ &\quad + \bar{E}_O(x,y)e^{j(\omega_O+\omega_{\rm rf})t}e^{-j\beta(\omega_O+\omega_{\rm rf})z}\\ &\quad \times e^{-\alpha(\omega_O+\omega_{\rm rf})z}. \end{aligned} \tag{1}$$

The total net optical power P_O flowing through a transverse plane in z results from the integration of Poynting vector $\overline{S_O}$ as follows:

$$\begin{aligned}P_O(z) &= \mathrm{Re}\left\{\int_A \overline{S_O}(x,y,z)\cdot\overline{dA}\right\}\\ &= \mathrm{Re}\left[\frac{1}{2}\int_A \left\{\overline{E_O}(x,y,z)\times\overline{H_O}^*(x,y,z)\right\}\cdot\overline{a_z}\,dA\right]\end{aligned} \tag{2}$$

where A is the transverse section of the equivalent line in abscissa z. The optical fields are assumed to have a quasi-TEM behavior with a real characteristic impedance $1/\eta$. Hence, after calculations, the traveling optical power associated with the total field is

$$P_O(z) = \mathrm{Re}\left\{\frac{1}{2}\int_A \eta|\bar{E}_1+\bar{E}_2|^2\,dA\right\} \tag{3a}$$

$$= P_O e^{-2\alpha(\omega_O)z}\left\{1 + e^{-\Delta\alpha z}\cos(\omega_{\rm rf}t - \Delta\beta z)\right\} \tag{3b}$$

with

$$\begin{aligned}P_O &\triangleq \int_A \eta|\overline{E_O}|^2\cdot\overline{dA}\\ &\triangleq \int_A \overline{S_O}(x,y)\cdot\overline{dA}\end{aligned} \tag{3c}$$

$$\begin{aligned}\Delta\alpha &\triangleq \alpha(\omega_O+\omega_{\rm rf}) - \alpha(\omega_O)\\ &= \left.\frac{\partial\alpha}{\partial\omega}\right|_{\omega_O}\omega_{\rm rf}\\ &= \frac{\hbar K^2}{4\pi q\alpha(\omega_O)}\omega_{\rm rf}\end{aligned} \tag{3d}$$

$$\begin{aligned}\Delta\beta &\triangleq \beta(\omega_O+\omega_{\rm rf}) - \beta(\omega_O)\\ &= \left.\frac{\partial\beta}{\partial\omega}\right|_{\omega_O}\omega_{\rm rf}\\ &= \frac{n_O\omega_{\rm rf}}{c}\end{aligned} \tag{3e}$$

$$\alpha(\omega) = K\sqrt{\left(\frac{\hbar\omega}{2\pi q}\right) - E_g} \tag{3f}$$

where

- K constant function of the electron and hole equivalent mass;
- $\hbar$ normalized Planck's constant;
- c speed of light in vacuum;
- n_O optical refractive index of medium guiding optical signal;
- E_g bandgap energy of the semiconductor considered.

The above linearizations are valid provided that the bandwidth of the modulating RF signal (maximum 200–300 GHz) remains small with respect to the optical carrier frequency (of the order of 200 THz). Equations (3d) and (3e) illustrate the fact that the microwave signal is submitted to the same optical steady-state phenomena as the carrier [8], including modal, material, and waveguide dispersion, as well as scattering and optical reflection from discontinuities that are of the order of the optical wavelength. The RF part of (3b) is the optical power scattering wave $p(z)$ we defined in [9] for optical ports of E/O and O/E transducers

$$p_{\rm rf}(z) = P_O e^{-2\alpha(\omega_O)z}e^{-\Delta\alpha + j\Delta\beta z}. \tag{4}$$

The attenuation denotes the conversion of optical power into a rate of generated carriers, as will be shown later.

2) Reflected Power Scattering Wave: Assuming a forward optical field

$$E^+(x,y,z) = E_O^+(x,y)e^{j\omega_O t}e^{-\gamma_O z}\left(1 + e^{j\omega_{\rm rf}t}e^{-\Delta\gamma z}\right)$$

with

$$\begin{aligned}\gamma_O &= \alpha_O + j\beta_O\\ &= \alpha(\omega_O) + j\beta(\omega_O)\\ \Delta\gamma &= \Delta\alpha + j\Delta\beta\end{aligned} \tag{5}$$

the field reflected at a load in z_L is a function of the various frequency components of the forward field. Its two parts, at ω_O

and $\omega_O+\omega_{\rm rf}$, respectively, propagate toward the input with their respective propagation constant

$$\begin{aligned} E^-(x,y,z) &= E_O^+(x,y)e^{j\omega_O t}\Big\{\Gamma_O(\omega_O)e^{-\gamma_O z_L}e^{-\gamma_O(z_L-z)} \\ &\quad +\Gamma_O(\omega_O+\omega_{\rm rf})e^{j\omega_{\rm rf}t}e^{-(\Delta\gamma+\gamma_O)z_L} \\ &\quad \times e^{-(\Delta\gamma+\gamma_O)(z_L-z)}\Big\} \end{aligned} \tag{6}$$

where Γ_O is the optical reflection coefficient at the load. When the bandwidth of the RF signal is small compared with the optical frequency, which is the usual case, the load can be considered as nondispersive with a constant magnitude at optical wavelengths, yielding

$$\Gamma_{\rm OL}(\omega) \triangleq |\Gamma_{\rm OL}|e^{j(\phi_{\rm OL}-\omega\tau)} \tag{7}$$

where τ is the group delay of the optical load. In that case, the reflected electric field (6) is rewritten using (7), and the total field $E_O^+ + E_O^-$ is used for deriving the total optical power P_O, using (3a) with subscripts "1" and "2" replaced by $+$ and $-$, respectively. Hence, extending definition (4), the total RF power scattering wave is the combination of forward and reflected power scattering waves

$$p_{\rm rf}(z) \triangleq p_{\rm rf}^+(z) - p_{\rm rf}^-(z) = p_{\rm rf}^+(z)\Big\{1-\Gamma_{{\rm rf}\,L}e^{2\gamma_{\rm rf}(z-z_L)}\Big\} \tag{8}$$

where

$$\Gamma_{{\rm rf}\,L} \triangleq |\Gamma_{\rm OL}|^2 e^{-j\omega_{\rm rf}\tau} \tag{9}$$

is the reflection factor relating $p_{\rm rf}^+$ and $p_{\rm rf}^-$ in $z = z_L$ with $\gamma_{\rm rf} \triangleq 2\alpha(\omega_O)+\Delta\alpha+j\Delta\beta$ propagation coefficient of power scattering wave (4). The reflection coefficient is similar to that obtained on a conventional transmission line.

B. Expression for RF Current Photo Induced in the p-i-n Photodetector

1) Equation for Distributed O/E Conversion: As usual for photodetectors, we neglect diffusion and recombination mechanisms. Each carrier current density is then proportional to the product of the carrier density by its velocity, and the well-known transport equations for electron and hole distributions simplify into

$$\begin{aligned} \frac{\partial n}{\partial t} &= -\nabla\cdot\bar{J}_n/q + G_n = -\nabla\cdot(n\bar{v}_n) + G_n \\ \frac{\partial p}{\partial t} &= +\nabla\cdot\bar{J}_p/q + G_p = -\nabla\cdot(p\bar{v}_p) + G_p \end{aligned} \tag{10}$$

where $G_{n,p}$ are the rates of generated carriers, and $\bar{v}_{n,p}$ their saturation velocities, where subscripts n and p refer to electrons and holes, respectively. Since the optical power P_O results from the integration (2) of the power density, optical power density scattering waves $s_{\rm rf}^{\pm}(\omega_{\rm rf},x,y,z)$ can be defined. The integral of $s_{\rm rf}^{\pm}$ over the transverse section of the p-i-n line yields the power scattering waves (8). The $s_{\rm rf}$ waves contribute to the rate of photogenerated carriers per unit volume by means of the field absorption coefficient $\alpha(\omega_O)$, which expresses the decrease of optical power due to carrier generation. Hence, it can easily be shown that the rate of generated carriers per unit volume (equal for electrons and holes because of conversion of photons into electron–hole pairs) is

$$G_{n,p}(\omega_{\rm rf}) = \frac{\alpha(\omega_O)}{\hbar\omega_O}\Big(s_{\rm rf}^+ + s_{\rm rf}^-\Big). \tag{11}$$

The velocities do not depend on position because the p-i-n junction is depleted and saturated. Hence, drift current occurs along the x-axis only: $v_{ny} = v_{nz} = 0$. Using (11), (10) then has as general RF solution for electron and holes current densities along the z-axis

$$\begin{aligned} J_{zn,p}(\omega_{\rm rf}) = -qv_{n,p}\big[\alpha(\omega_O)/\hbar\omega_O\big] \times \int e^{j\omega_{\rm rf}(x-x')/v_{n,p}} \\ \times\Big\{s_{\rm rf}^+(\omega_{\rm rf},x') + s_{\rm rf}^-(\omega_{\rm rf},x')\Big\}dx'. \end{aligned} \tag{12}$$

2) Distributed RF Photogenerated Current: The knowledge of the transverse dependence $S_O(x,y)$ of the optical power densities yields the distribution of photogenerated current densities (12) in the intrinsic area. The particular case of a Dirac impulse in $x=0$, uniform along the y-axis in the intrinsic area, is often considered as follows:

$$S_O(x,y) = (P_O/d_{\rm intr})\delta(x). \tag{13}$$

The total current collected at one of the electrodes results from the integration in $x = L_{\rm intr}/2$ of the current densities (12) over the width $d_{\rm intr}$ of the intrinsic area, which yields

$$\begin{aligned} j(z,\omega_{\rm rf}) = q\big[\alpha(\omega_O)/\hbar\omega_O\big]\big(e^{j\omega_{\rm rf}\tau_n/2}+e^{j\omega_{\rm rf}\tau_p/2}\big) \\ \times\big[p_{\rm rf}^+(\omega_{\rm rf},z)+p_{\rm rf}^-(\omega_{\rm rf},z)\big] \end{aligned} \tag{14}$$

where $\tau_{n,p}$ is the carrier transit time. When considering $L_{\rm intr}$ small with respect to $v_{n,p}$, yielding a zero equivalent transit time, and for a structure having only a forward optical propagation ($p_{\rm rf}^- = 0$), (14) is in accordance with the O/E equation proposed by Hielata in [11] for uniform illumination. Obviously, more complicated distributions $S_O(x,y)$ can be taken into account in our model.

C. RF Infinitesimal Equivalent Circuit for Forward Detection Mode

In each abscissa z, we consider the photogenerated current (14) as a source of current per unit length [12], [13]. It divides itself between the input impedances $Z_{\rm in}$ of the left-hand-side section of length z loaded by Z_{LE1}, and $Z_{\rm out}$ of the right-hand-side section of length $(L_{\rm pin}-z)$ loaded by Z_{LE2}. Currents and voltages at each electrical port can easily be expressed as a function of the source $j(z,\omega)\,dz$ induced by an illumination over infinitesimal length dz in abscissa z, using a chain matrix formalism [12]

$$\begin{aligned} dV_{\rm in,out} &= \Big[T_{11{\rm in,out}}Z_{\rm in}(z,\omega_{\rm rf})Z_{\rm out}(z,\omega_{\rm rf}) \\ &\quad + T_{12{\rm in,out}}Z_{\rm out,in}(z,\omega_{\rm rf})\Big] \\ &\quad \times j(z,\omega_{\rm rf})\,dz/(Z_{\rm in}+Z_{\rm out}) \\ dI_{\rm in,out} &= \Big[T_{21{\rm in,out}}Z_{\rm in}(z,\omega_{\rm rf})Z_{\rm out}(z,\omega_{\rm rf}) \\ &\quad + T_{22{\rm in,out}}Z_{\rm out,in}(z,\omega_{\rm rf})\Big] \\ &\quad \times j(z,\omega_{\rm rf})\,dz/(Z_{\rm in}+Z_{\rm out}) \end{aligned} \tag{15}$$

where $T_{ij\,\mathrm{in}}$ are the elements of the 2×2 inverse of the chain matrix of the p-i-n line of length $(L_{\mathrm{pin}} - z)$, while $T_{ij\,\mathrm{out}}$ are the elements of the 2×2 chain matrix of the p-i-n line of length z. We have established efficient formulations of transmission-line parameters γ, Z_c for each of the two p-i-n lines (Fig. 1) [13], [14]. They are used here for the calculation of $T_{ij\,\mathrm{in,out}}$ and $Z_{\mathrm{in,out}}$. Integrating the contributions of the infinitesimal source $j(z,\omega)\,dz$ finally yields voltage $V_{\mathrm{in,out}}$ and current $I_{\mathrm{in,out}}$ at input and output electrical ports, respectively; hence, the RF power $P_{\mathrm{forw\,rf}}$ delivered at each E-port as follows:

$$\begin{aligned} V_{\mathrm{in,out}} &= \int_0^{L_{\mathrm{pin}}} dV_{\mathrm{in,out}}(z)\,dz, \\ I_{\mathrm{in,out}} &= \int_0^{L_{\mathrm{pin}}} dI_{\mathrm{in,out}}(z)\,dz \\ P_{\mathrm{forw\,rf\,in,out}} &= \frac{1}{2} V_{\mathrm{in,out}} I^*_{\mathrm{in,out}}. \end{aligned} \tag{16}$$

Thus, the power delivered to the RF loads is expressed as a function of the current density (14) using (15); hence, as a function of the power scattering waves $p^{+,-}_{\mathrm{rf}}\cdot$.

IV. Equivalent Circuits for Reverse Emission Mode

A. Equivalent RF Impedance for Laser Junction

The equations governing the laser operation mode of the diode are reported in [15]. We linearize them for obtaining their RF parts as

$$\begin{aligned} &j\omega_{\mathrm{rf}} n + \frac{n}{\tau_s} + \frac{N_{\mathrm{ph}}}{\tau_s} n + \frac{(N - N_m)}{\tau_{\mathrm{ph}}} n_{\mathrm{ph}} \\ &\quad = \frac{i_{\mathrm{bias}}(\omega_{\mathrm{rf}})}{qad} \end{aligned} \tag{17a}$$

$$\begin{aligned} &j\omega_{\mathrm{rf}} n_{\mathrm{ph}} + \frac{n_{\mathrm{ph}}}{\tau_{\mathrm{ph}}} - \beta \frac{n}{\tau_s} - \frac{N_{\mathrm{ph}}}{\tau_s} n - \frac{(N - N_m)}{\tau_{\mathrm{ph}}} n_{\mathrm{ph}} \\ &\quad = 0 \end{aligned} \tag{17b}$$

with n and n_{ph} electrons and photons densities, respectively, $i_{\mathrm{bias}}(\omega_{\mathrm{rf}})$ RF biasing currrent, a area of the junction, d_{intr} its thickness, q electron charge, N_m normalized steady-state value of minimum electron density required to obtain laser gain, N and N_{ph} normalized steady-state values of electron and photon densities, respectively, and τ_s and τ_{ph} lifetimes of electrons and photons, respectively. Using those equations, the equation for the RF equivalent impedance $Z_{\mathrm{las}}(\omega_{\mathrm{rf}})$ of the laser junction of section $(L_{\mathrm{pin}}\, L_{\mathrm{intr}})$ is determined as in [15].

B. Equivalent Infinitesimal Circuit for RF Signal Biasing Equivalent Laser Junction

The laser emission effect is introduced in the RF equivalent circuit of the emission mode by adding the infinitesimal laser admittance $1/z_{\mathrm{las}} = 1/L_{\mathrm{pin}} Z_{\mathrm{las}}(\omega_{\mathrm{rf}})$ with the parallel infinitesimal admittance of the equivalent p-i-n RF transmission line. Noting γ_{las} and Z_{clas}, the RF parameters of the p-i-n photodetector taking this laser effect into account, and γ and Z_c those computed for the nonemitting structure, we have

$$\begin{aligned} \gamma_{\mathrm{las}} &= \sqrt{Z[Y + 1/Z_{\mathrm{las}}]} \\ Z_{\mathrm{clas}} &= \sqrt{Z/[Y + 1/Z_{\mathrm{las}}]} \end{aligned} \tag{18}$$

with

$$\begin{aligned} Z &= \gamma(\omega_{\mathrm{rf}}) Z_c(\omega_{\mathrm{rf}}) \\ Y &= \gamma(\omega_{\mathrm{rf}}) / Z_c(\omega_{\mathrm{rf}}). \end{aligned}$$

The emission mode is thus characterized by a line of length L_{pin}, fed by an RF signal at frequency ω_{rf} in abscissa $z = L_{\mathrm{pin}}$, and loaded by an impedance Z_{LE1} in $z = 0$. The current and voltage on this equivalent line are easily obtained from the classical transmission-line formalism for forward and reverse waves as a function of the RF biasing voltage V_{E2} or current I_{E2} imposed at port $E2$ $(z = L_{\mathrm{pin}})$ with

$$\Gamma_{E1} = \frac{Z_{LE1} - Z_{\mathrm{clas}}}{Z_{LE1} + Z_{\mathrm{clas}}} \tag{19}$$

describing the RF behavior of reflection coefficient of load at port $E1$.

C. Modulated Part of the Emitted Optical Power

From (17a) and (17b), it is easy to deduce the relationship between the RF variation $j\omega_{\mathrm{rf}} n_{\mathrm{ph}}$ of the photon density and the biasing current per unit length $i_{\mathrm{bias}}(\omega_{\mathrm{rf}})$. The relationship between n and the voltage $v(\omega_{\mathrm{rf}})$ across the diode is indeed

$$n = (\tau_s / qR_d) v(\omega_{\mathrm{rf}}) = (\tau_s / qR_d) Z_{\mathrm{las}}(\omega_{\mathrm{rf}}) i_{\mathrm{bias}}(\omega_{\mathrm{rf}}) \tag{20}$$

while (17b) yields a straightforward relationship between n_{ph} and n. Introducing (20) into (17b) and rearranging yields the rate of photons g_{ph}

$$\begin{aligned} g_{\mathrm{ph}}(\omega_{\mathrm{rf}}) &= j\omega_{\mathrm{rf}} n_{\mathrm{ph}} \\ &= (j\omega_{\mathrm{rf}} \tau_s / qR_d) \\ &\quad \times \frac{z_{\mathrm{las}}(\omega_{\mathrm{rf}}) i_{\mathrm{bias}}(\omega_{\mathrm{rf}}) \left(\dfrac{\beta}{\tau_s} + \dfrac{N_{\mathrm{ph}}}{\tau_s} \right)}{j\omega_{\mathrm{rf}} + \dfrac{1}{\tau_{\mathrm{ph}}} - \dfrac{(N - N_m)}{\tau_{\mathrm{p}}}}. \end{aligned} \tag{21}$$

The infinitesimal equivalent source of RF modulation for optical power emitted in z is

$$dp_{\mathrm{rf}}(\omega_{\mathrm{rf}}, z) = (L_{\mathrm{intr}}\, d_{\mathrm{intr}}) \hbar \omega_O g_{\mathrm{ph}}(\omega_{\mathrm{rf}}) \tag{22}$$

where $i_{\mathrm{bias}}(\omega_{\mathrm{rf}})$ is the fraction of current responsible for the laser effect, flowing into the impedance $z_{\mathrm{las}}(\omega_{\mathrm{rf}})$. It is proportional to the total RF voltage $V_{\mathrm{rev}}(z)$ traveling on the line

$$i_{\mathrm{bias}}(\omega_{\mathrm{rf}}) = V_{\mathrm{rev}}(z) / Z_{\mathrm{las}}(\omega_{\mathrm{rf}}). \tag{23}$$

Inserting (23) in (21) finally yields the relationship between the rate of generated photons g_{ph} and the RF voltage on the p-i-n line; hence, between dp_{rf} and $V_{\mathrm{rev}}(z)$, using (22). Assuming that the modulated part of the emitted optical power splits into two equal parts traveling in opposite directions, the optical power at ports $O1$ and $O2$ results from the optical distributed source $dp_{\mathrm{rf}}(\omega_{\mathrm{rf}}, z)$ as

$$\begin{aligned} dp_{\mathrm{las}\,O1} &= \frac{dp_{\mathrm{rf}}(\omega_{\mathrm{rf}}, z)}{2} e^{-j\Delta\beta z} \\ &\quad \times \left[1 - \Gamma_{\mathrm{rf}\,O2} e^{-j2\Delta\beta(L_{\mathrm{pin}} - z)} \right] dz \\ dp_{\mathrm{las}\,O2} &= \frac{dp_{\mathrm{rf}}(\omega_{\mathrm{rf}}, z)}{2} e^{-j\Delta\beta(L_{\mathrm{pin}} - z)} [1 - \Gamma_{\mathrm{rf}\,O2}]\, dz \end{aligned} \tag{24}$$

where $\Gamma_{\mathrm{rf}\,O2}$ is the reflection coefficient associated with the RF modulating part of the optical power at port $O2$. Integrating (24) over z yields the total power $p_{\mathrm{las}\,O1,O2}$ at input and output

$$p_{\mathrm{las}\,O1,O2} = \int_0^{L_{\mathrm{pin}}} dp_{\mathrm{las}\,O1,O2}(z)\,dz. \tag{25}$$

V. Scattering Matrix

A. Definition of Scattering Waves

Scattering waves are defined at optical and electrical ports according to our definition [9].

1) Forward Photodetection Mode: Scattering waves at optical ports are obtained from power scattering waves [see (8) and –(9)] by terminating port $O2$ by a reflection coefficient $\Gamma_{\mathrm{rf}\,O2}$, (9) measuring the effect on the RF modulating part of optical power

$$\begin{aligned} a_{\mathrm{forw}O1} &= p_{\mathrm{rf}}^{+}(0) = P_O \\ b_{\mathrm{forw}O1} &= p_{\mathrm{rf}}^{-}(0) = \Gamma_{\mathrm{rf}\,O2} P_O e^{-2\gamma_{\mathrm{rf}O} L_{\mathrm{pin}}}. \end{aligned} \tag{26}$$

The optical power transmitted at $O2$ is the scattering wave $b_{\mathrm{forw}\,O2}$ while the wave reflected at this port is the scattering wave $a_{\mathrm{forw}\,O2}$. The RF scattering waves at input and output are obtained from voltages and currents $V_{\mathrm{in,out}}$ and $I_{\mathrm{in,out}}$ at those accesses loaded by impedances Z_{LE1} and Z_{LE2}, respectively. They are obtained by using (15) and (16), as explained in Section III-C. At electrical ports $E1$ and $E2$, they result from the classical network theory [10].

2) Reverse Emission Mode: The RF scattering waves are defined as usual. On the other hand, the modulated part (25) of optical power induced by biasing RF current $i_{\mathrm{bias}}(\omega_{\mathrm{rf}})$ is the outgoing optical scattering wave emitted at port $O1$ supposed to be optically matched ($\Gamma_{\mathrm{rf}O1} = 0$). The forward term of (25) taken at port $O2$ is the power scattering wave $a_{\mathrm{rev}\,O2}$ reflected at port $O2$, while the reverse term is the outgoing power scattering wave $b_{\mathrm{rev}\,O2}$ emitted at port $O2$.

B. Scattering Matrix of the Four-Port O/E Converter

The scattering matrix of the equivalent four-port transducer [see Fig. 1(c)] is defined as

$$\begin{bmatrix} b_{O1} \\ b_{O2} \\ b_{E1} \\ b_{E2} \end{bmatrix} = \bar{\bar{S}}_{4-\mathrm{port}} \begin{bmatrix} a_{O1} \\ a_{O2} \\ a_{E1} \\ a_{E2} \end{bmatrix} \triangleq \begin{bmatrix} S_{O1O1} & S_{O1O2} & S_{O1E1} & S_{O1E2} \\ S_{O2O1} & S_{O2O2} & S_{O2E1} & S_{O2E2} \\ S_{E1O1} & S_{E1O2} & S_{E1E1} & S_{E1E2} \\ S_{E2O1} & S_{E2O2} & S_{E2E1} & S_{E2E2} \end{bmatrix} \begin{bmatrix} a_{O1} \\ a_{O2} \\ a_{E1} \\ a_{E2} \end{bmatrix}. \tag{27}$$

Each parameter S_{ij} is equal to the reverse scattering wave b_i obtained at port i when feeding only port j by a forward scattering wave a_j of unit magnitude, and matching all others ports ($i \neq j$). As an example, S_{E2O1} is the reverse scattering wave b_{E2} observed at $E2$ when port $O1$ is fed by a forward scattering wave a_{O1} of unit magnitude, and when ports $O2$ and $E1$ are matched. Due to the symmetry of the structures investigated here, only eight parameters have to be determined: S_{O1O1}, S_{O2O1}, S_{E2O1}, S_{E1O1}, S_{O1E2}, S_{O2E2}, S_{E2E2}, and S_{E1E2}. As stated in Section II, the four-port scattering matrix has particular properties resulting from physical symmetry with respect to the plane $z = L_{\mathrm{pin}}/2$. This symmetry implies that identical reference loads have to be used at ports $E1$ and $E2$, $O1$, and $O2$, respectively, to ensure matching when calculating a specific S_{ij}. Due to traveling mechanisms occuring on optical and electrical paths, matching E/O_j when E/O_i is fed implies that E/O_i is matched. Hence, the scattering matrix is that of a matched four-port ($S_{ii} = 0$).

1) Expressions for S_{O1O1}, S_{O2O1}, S_{E2O1}, and S_{E1O1}: Those parameters are calculated assuming that optical port $O1$ is fed by a forward scattering wave a_{O1} of unit magnitude and that no other forward scattering wave is present as follows:

$$a_{O1} = 1 \quad a_{O2} = a_{E1} = a_{E2} = 0. \tag{28}$$

Also, port $O2$ is matched or perfectly radiating so that no optical power is reflected. Furthermore, reference impedances at ports $E1$ and $E2$ must be equal to the RF characteristic impedance Z_c. By doing so, the RF signals generated on the p-i-n line are not reflected at the ports and the scattering waves a_{E1} and a_{E2} vanish. Hence, the reflection coefficient S_{O1O1} at port $O1$ and the transmission coefficient S_{O2O1} from $O1$ to $O2$ of modulating power are

$$S_{OkO1} = \left.\frac{b_{\mathrm{forw}Ok}}{a_{\mathrm{forw}O1}}\right|_{\Gamma_{\mathrm{rf}O2}=0}, \qquad \text{with } k = 1,2 \tag{29}$$

resulting in $S_{O1O1} = 0$. Similarly, the following conditions hold at ports $E1, E2$

$$Z_{LE1} = Z_{LE2} = Z_c \tag{30}$$

which yields

$$S_{EkO1} = \left.\frac{b_{\mathrm{forw}Ek}}{a_{\mathrm{forw}O1}}\right|_{\Gamma_{\mathrm{rf}O2}=0, Z_{LEk}=Z_c}, \qquad \text{with } k = 1,2 \tag{31}$$

2) Expressions for S_{O2E2}, S_{O1E2}, S_{E2E1}, and S_{E1E1}: Those parameters are calculated assuming that RF port $E2$ is fed by a unitary electrical scattering wave a_{E2} and that no other forward electrical and optical scattering wave is present as follows:

$$a_{E2} = 1 \quad a_{O1} = a_{O2} = a_{E1} = 0. \tag{32}$$

At RF ports $E1, E2$, conditions (30) and (32) must hold, which implies $\Gamma_{E1} = 0$. The reverse electrical parameters are

$$S_{EkE2} = \left.\frac{b_{\mathrm{rev}E2}}{a_{\mathrm{rev}E2}}\right|_{\Gamma_{E1}=0}, \qquad \text{with } k = 1,2 \tag{33}$$

resulting in $S_{E2E2} = 0$. At optical ports $O1$, $O2$, conditions (30) and (32) must hold, which implies $\Gamma_{\mathrm{rf}\,O2} = 0$ to cancel reflected power scattering waves, and $\Gamma_{E1} = 0$, yielding the reverse optical parameters

$$S_{OkE2} = S_{O2Ek} = \left.\frac{b_{\mathrm{rev}Ok}}{a_{\mathrm{rev}E2}}\right|_{\Gamma_{\mathrm{rf}O2}=0, \Gamma_{E1}=0}, \qquad \text{with } k = 1,2. \tag{34}$$

3) Expressions for S_{O2E1}, S_{O2E2}, S_{E2E1}, S_{E2E2}, S_{O1O1}, S_{O1O2}, S_{E1O1}, S_{E1O2}: By virtue of the symmetry of geometry and loads with respect to the plane $z = L_{\rm pin}/2$, the other coefficients of the S-matrix (27) are obtained as

$$\begin{aligned} S_{O2Ek} &= S_{OkE2} \\ S_{E2Ek} &= S_{EkE2} \\ S_{O1Ok} &= S_{OkO1} \\ S_{E1Ok} &= S_{EkO1}, \qquad \text{with } k = 1, 2. \end{aligned} \tag{35}$$

C. Reduction to Scattering Matrices of Three-Port O/E Converter

The reduction of the four-port scattering matrix into a three-port matrix describing the usual mode of operation of TWPD's is readily obtained by imposing that electrical port $E1$ is open ($\Gamma_{E1} = 1$). The scattering matrix of the equivalent three-port transducer is then

$$\begin{bmatrix} b_{O1} \\ b_{O2} \\ b_{E2} \end{bmatrix} = \bar{\bar{S}}_{3-\rm port} \begin{bmatrix} a_{O1} \\ a_{O2} \\ a_{E2} \end{bmatrix} \triangleq \begin{bmatrix} S_{O1O1} & S_{O1O2} & S_{O1E2} \\ S_{O2O1} & S_{O2O2} & S_{O2E2} \\ S_{E2O1} & S_{E2O2} & S_{E2E2} \end{bmatrix} \begin{bmatrix} a_{O1} \\ a_{O2} \\ a_{E2} \end{bmatrix}. \tag{36}$$

The coefficients are obtained from previous expressions, where condition $\Gamma_{E1} = 0$ is replaced by condition $\Gamma_{E1} = 1$, and condition $Z_{LE1} = Z_c$ is replaced by condition $1/Z_{LE1} = 0$. Expressions for coefficients not involved in (36) are irrelevant. Another reduction occurs when optical port $O2$ is open, with a total reflection of optical beam at output, which yields

$$\begin{bmatrix} b_{O1} \\ b_{E1} \\ b_{E2} \end{bmatrix} = \bar{\bar{S}}_{3-\rm port} \begin{bmatrix} a_{O1} \\ a_{E1} \\ a_{E2} \end{bmatrix} \triangleq \begin{bmatrix} S_{O1O1} & S_{O1E1} & S_{O1E2} \\ S_{E2O1} & S_{E1E1} & S_{E1E2} \\ S_{E1O1} & S_{E2E1} & S_{E2E2} \end{bmatrix} \begin{bmatrix} a_{O1} \\ a_{E1} \\ a_{E2} \end{bmatrix}. \tag{37}$$

Coefficients of this three-port S-matrix are also obtained from previous expressions, where condition $\Gamma_{{\rm rf}\,O2} = 0$ is replaced by condition $\Gamma_{{\rm rf}\,O2} = 1$. Expressions for coefficients not involved in (37) are irrelevant.

D. Reduction to Scattering Matrices of Two-Port O/E Converter

A further reduction combines the open-ended condition at both optical port $O2$ and RF port $E1$, yielding the two-port scattering matrix of the O/E converter

$$\begin{bmatrix} b_{O1} \\ b_{E2} \end{bmatrix} = \bar{\bar{S}}_{2-\rm port} \begin{bmatrix} a_{O1} \\ a_{E2} \end{bmatrix} \triangleq \begin{bmatrix} S_{O1O1} & S_{O1E2} \\ S_{E2O1} & S_{E2E2} \end{bmatrix} \begin{bmatrix} a_{O1} \\ a_{E2} \end{bmatrix}. \tag{38}$$

Coefficients of this two-port S-matrix are again obtained from previous expressions, where condition $\Gamma_{E1} = 0$ is replaced by condition $\Gamma_{E1} = 1$, condition $Z_{LE1} = Z_c$ by condition $1/Z_{LE1} = 0$, and condition $\Gamma_{{\rm rf}\,O2} = 0$ by condition $\Gamma_{{\rm rf}\,O2} = 1$. Definitions of coefficients not involved in (38) are again irrelevant.

VI. Validation and Bandwidth Limitations

A. Four-Port Configurations

1) Infinitely Long TWPD: Fig. 2 shows the nonzero parameters of the scattering matrix for a mesa TWPD with the configuration proposed by Hielata [11]. The device is of GaAs type, with a length $L_{\rm pin} = 500$ μm. The width of its intrinsic area is 2 μm, and its thickness 3.17 μm. The wavelength of optical carrier is 1.06 μm, and the field absorption coefficient $\alpha(\omega_O)$ is 50 cm^{-1}. The device is very long, and the TWPD can be considered as infinitely long, as in [11]. The illumination mode is uniform, which means $\tau_{n,p} = 0$ in (14). It is further assumed that RF losses are negligible, characteristic impedance of the TWPD is 50 Ω, and the electrical ports $E1$ and $E2$ are loaded by 50 Ω

$$\Gamma_{E1} = \frac{Z_{\rm in} - Z_c}{Z_{\rm in} + Z_c} = \Gamma_{E2} = \frac{Z_{\rm out} - Z_c}{Z_{\rm out} + Z_c} = 0. \tag{39}$$

Output $O2$ is assumed to be optically matched: $\Gamma_{{\rm rf}\,O2} = 0$. The structure is thus depicted by the four-port configuration discussed in Section V-B. Fig. 2 shows results calculated with our model. Fig. 2(a) shows the optical transmission between ports $O1$ and $O2$. Due to the very long structure, most of the modulated optical power is converted into electrical currents along the length, and the residual fraction of optical power incoming at port $O2$ is very small. It varies slowly with frequency, confirming the fact that the frequency dependence of the field absorption coefficient is negligible over bandwidths smaller than 300 GHz. Fig. 2(c) shows the scattering parameters S_{E2O1} and S_{E1O1} (31) expressing the O/E conversion. They are compared with the scattering parameter associated to an "ideal" photodetector (curve noted "ideal PD"), in which delays induced by optical and RF propagation are neglected, as well as carrier transit times in the structure. Thus, the photogenerated current at output E is given by the simplified O/E balance equation

$$i_E = \frac{q}{\hbar\omega_O} p \triangleq K_{O/E} p \tag{40}$$

which yields the $S_{E2O1\,\rm ideal}$ of the ideal PD

$$\begin{aligned} S_{E2O1\,\rm ideal} &= \frac{b_{{\rm forw}E}}{a_{{\rm forw}O}} \\ &= \frac{\sqrt{\mathrm{Re}\, Z_c} i_E}{p} \\ &= \frac{q}{h\omega_O} \sqrt{\mathrm{Re}\, Z_c} \\ &= K_{O/E} \sqrt{\mathrm{Re}\, Z_c}. \end{aligned} \tag{41}$$

The figure shows that the ideal O/E conversion is wide band, as well as the O/E conversion S_{E2O1} between ports $O1$ and $E2$. This is because velocity matching is achieved between the RF modulation and photogenerated RF signal: the phases of this conversion scattering parameter [see Fig. 2(g)] and of the optical transmission factor S_{O2O1} [see Fig. 2(e)] are identical over the whole frequency range. Since the O and E signals travel in the same direction at the same velocity, a constructive interference occurs along the line between RF signals generated earlier on the line and those photogenerated in abscissa z, yielding no bandwidth limitation. This is not the case, however, for the fraction of photogenerated signal, which travels in the opposite

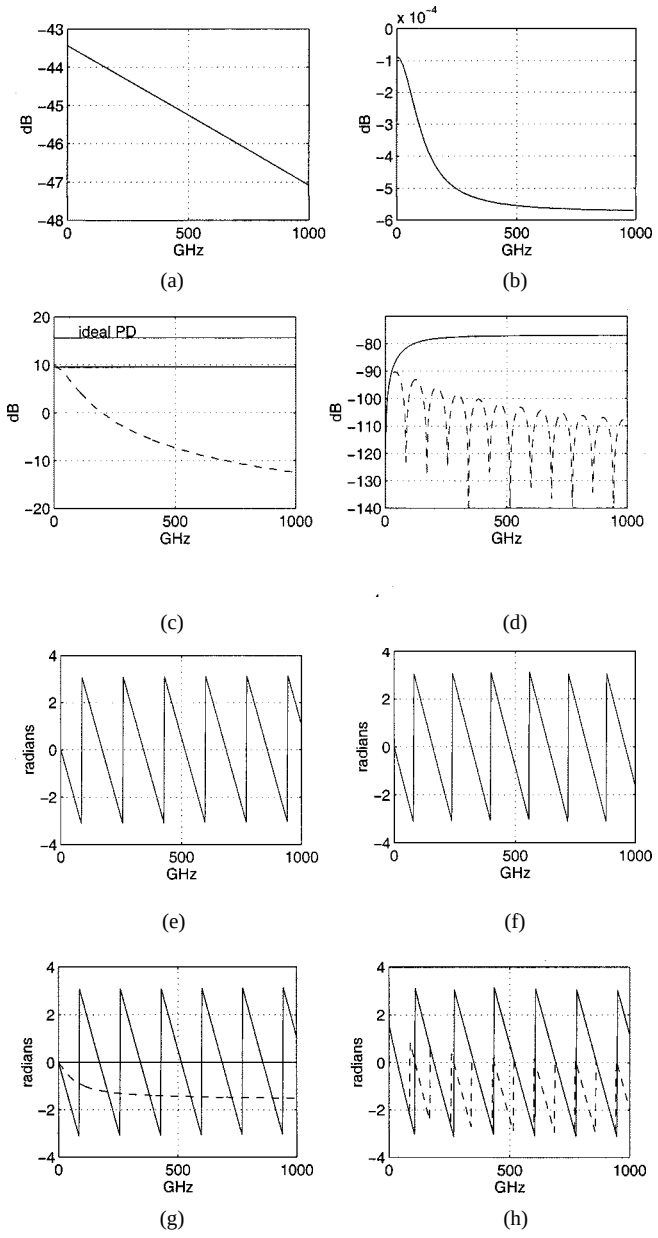

Fig. 2. Relevant parameters of four-port scattering matrix for a GaAs TWPD ($L_{\rm pin} = 500\ \mu$m, width of intrinsic area 2 μm, thickness 3.17 μm, wavelength of optical carrier 1.06 μm, field absorption coefficient 50 cm^{-1}). (a) Magnitude of O/O transmission (S_{O2O1}). (b) Magnitude of E/E transmission (S_{E1E2}). (c) Magnitude of O/E conversion [S_{E2O1} (—), (S_{E1O1}) (- -)]. (d) Magnitude of E/O conversion [S_{O1E2} (—), (S_{O2E2}) (- -)]. (e) Phase of O/O transmission (S_{O2O1}). (f) Phase of E/E transmission (S_{E1E2}). (g) Phase of O/E conversion [S_{E2O1} (—), (S_{E1O1}) (- -)]. (h) Phase of E/O conversion [S_{O1E2} (—), (S_{O2E2}) (- -)].

direction toward input $E1$: destructive interference occurs when frequency increases because of the increasing phase shift between the two signals, and the bandwidth of S_{E1O1} decreases [see Fig. 2(c)].

Concerning the reverse emission mode, the laser effect is of very low intensity since the E/O conversion observed between port $E2$ and optical ports $O1$ (S_{O1E2}) and $O2$ (S_{O2E2}) is very small [see Fig. 2(d)]. As a consequence, the RF transmission line is similar to an almost lossless matched transmission line, with nearly zero input reflection coefficient (S_{E2E2}, not shown) and nearly perfect transmission [see S_{E1E2} in Fig. 2(b)]. The

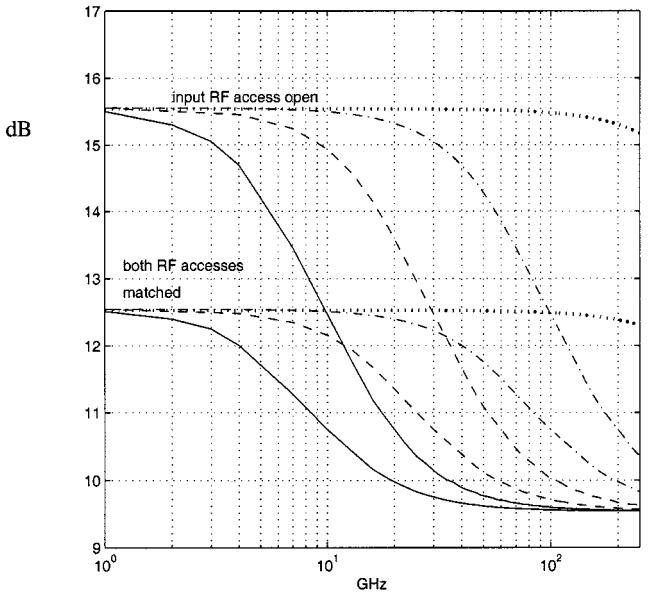

Fig. 3. Total RF power at output of TWPD in specific configuration [11, Fig. 4], computed by our four-port scattering model with $\alpha(\omega_O) = 5$ cm^{-1} (solid), 15 cm^{-1} (dashed), 50 cm^{-1} (dot-dashed) and 500 cm^{-1} (dotted), and two different load conditions at input electrical port $E1$: matched (lower curves) and open-circuit (upper curves).

slight decrease in magnitude is due to the losses induced by the weak laser emission effect. A destructive interference is also observed on S_{O2E2} because of RF signal and modulated optical power traveling in opposite directions. The frequency behavior of the O/E scattering parameters S_{E2O1} and S_{E1O1} is in accordance with that observed by Hielata. The validity of our model is illustrated in Fig. 3, showing the total RF power resulting from O/E conversion, computed for four values of $\alpha(\omega_O) = 5$, 15, 50, and 500 cm^{-1}. The model yields the total RF power collected at the electrical ports, defined as

$$10\log_{10}\left(|S_{E2O1}|^2 + |S_{E1O1}|^2\right). \tag{42}$$

Our results (lower curves in Fig. 3) perfectly agree with those by Hielata [11, Fig. 4]. At low frequencies, the total O/E conversion (42) is 12.6 dB and exhibits a 3-dB drop when compared to the 15.6 dB of the ideal case [see Fig. 2(c)]. This is because only half the total photogenerated current is collected in each port $E1$ and $E2$. At high frequencies, the total O/E conversion (42) undergoes a rolloff phenomenon induced by the behavior of $|S_{E1O1}|$ [see Fig. 2(c)], which is due to destructive interferences. Again magnitude, slope, and dependence with respect to $\alpha(\omega_O)$ calculated with our model confirm those by Hielata.

2) Conservation Law for the Four-Port S-Matrix of a Detector: The scattering parameters of microwave passive lossless four-port obey the conservation law

$$|S_{1j}|^2 + |S_{2j}|^2 + |S_{3j}|^2 + |S_{4j}|^2 = 1. \tag{43}$$

Multiplying (43) by $|a_{Ej}|^2$ yields

$$|b_{E1j}|^2 + |b_{E2j}|^2 + |b_{E3j}|^2 + |b_{E4j}|^2 = |a_{Ej}|^2. \tag{44}$$

For an O/E detector, a conservation law occurs only between optical power and photogenerated electrical current, which are related by a conversion factor $K_{O/E}$, as seen in (14) for the

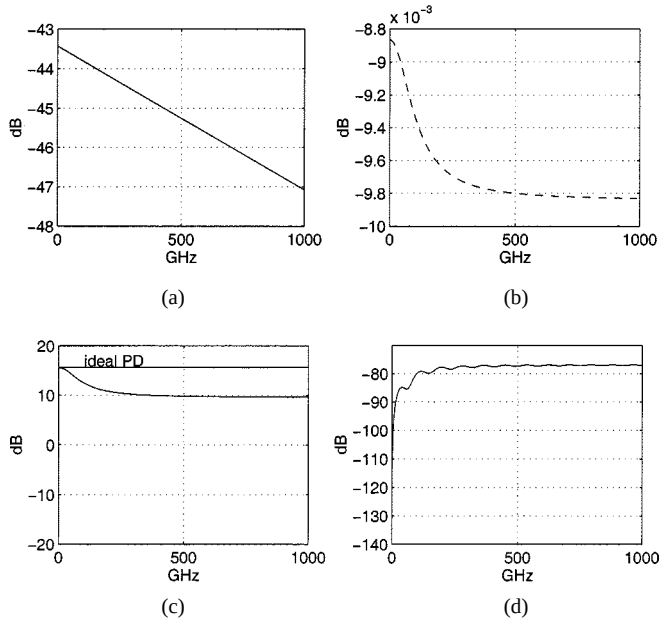

Fig. 4. Scattering parameters of a three-port, with configuration as in Fig. 2 ($L_{\rm pin} = 500\ \mu$m), except for $1/Z_{LE1} = 0$. (a) S_{O2O1}. (b) S_{e2e2}. (c) S_{E2O1}. (d) [S_{O1E2} (—), (S_{O2E2}) (- -)].

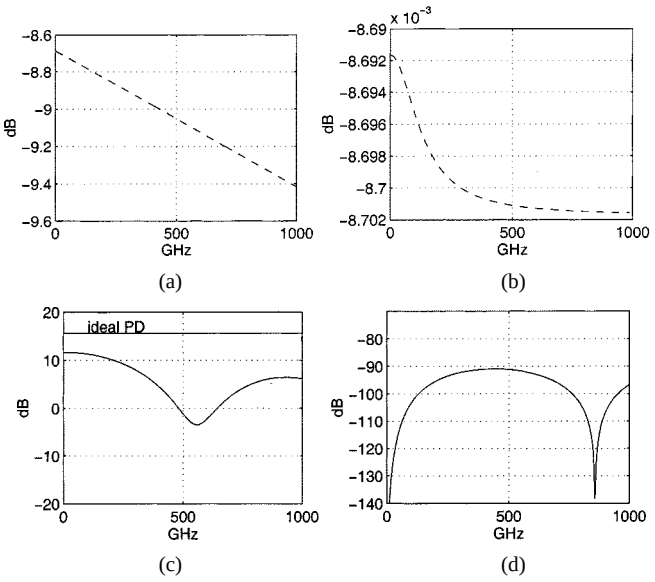

Fig. 5. Scattering parameters of two-port, with configuration as in Fig. 2, except for $L_{\rm pin} = 50\ \mu$m, $\Gamma_{{\rm rf}\,O1} = 0$, and $1/Z_{LE1} = 0$. (a) S_{O1O1}. (b) S_{E2E2}. (c) S_{E2O1}. (d) S_{O1E2}.

TWPD case and (40) for the ideal case. As a consequence, a hybrid balance equation can be written between the infinitesimal power scattering wave and the electrical current (14)

$$dp_O(z) = (1/K_{O/E})(dj_{{\rm forw}\,E1} + dj_{{\rm forw}\,E2}) \qquad (45)$$

where $j_{{\rm forw}\,E1}$ and $j_{{\rm forw}\,E2}$ are the fractions of current (14) flowing into input impedances $Z_{\rm in}$ and $Z_{\rm out}$, respectively. If the TWPD is electrically short, the total current collected at each electrical port is simply proportional to the length of the TWPD. The integrated equations between the power scattering wave and the electrical waves then yield

$$1 = S_{O1O1} + S_{O2O1} + (S_{E1O1} + S_{E2O1})/\sqrt{Z_c}K_{O/E}. \qquad (46)$$

Adequate equations for the three- and two-port configurations are easily deduced by cancelling the irrelevant scattering parameters in (46). We have calculated the value of the right-hand side of (46) for the various four-, three-, and two-port configurations. It is in the range 0.999 : 1 for lossless cases, which confirms the validity of the conservation law (46).

B. Three-Port Configurations

Fig. 4 shows scattering-parameter magnitudes of the three-port configuration defined in Section V-C. The TWPD is very long as in Section VI-A.1. However, the *input electrical port $E1$ is left open*. For the emission mode, it is obvious that the reflection coefficient S_{E2E2} has a magnitude close to one because of the open end $E1$, with a slight decrease along the line due to the losses induced by the weak laser emission effect. A standing wave pattern occurs along the electrical path, which implies that the optical power is emitted with the same phase along the line. Hence, no destructive interference occurs, and integrating along the length yields scattering parameters S_{E1O1} and S_{E2O1} of equal magnitude [superimposed in Fig. 4(d)].

For the O/E conversion, the photogenerated RF signal traveling toward the input is totally reflected at $E1$, and finally collected at $E2$, yielding S_{E2O1} as the sum of the forward and reflected signals. At low frequencies, no destructive interference occur, and RF photogenerated voltages and currents are in phase at output, yielding ideal conversion. At higher frequencies, S_{E2O1} is close to the sum of square magnitudes of S_{E2O1} and S_{E1O1} of the matched case depicted in Fig. 2(c), and S_{E2O1} decreases rapidly with frequency, as S_{E1O1} of the matched case. This is also observed on the E/O conversion [see Fig. 4(d)]. The behavior of S_{E2O1} is in accordance with [11] for the same three-port configuration. The total RF power (42), computed using our three-port formalism with the four same different values of α, is identical in this case to the sole S_{E2O1}. It shows again a perfect agreement (Fig. 3, upper curves) with previously published results [11]. At low frequency, the total O/E conversion S_{E2O1} is 15.6 dB, as in the ideal case. At high frequency, the total RF power has the same magnitude, slope, and dependence to α, as in [11, Fig. 4]. The rolloff is due to the decrease with frequency of S_{E2O1}, illustrated in Fig. 4(c).

When a length reduction occurs in this three-port configuration ($L_{\rm pin} = 50\ \mu$m), O/E conversion is only partial, the emission parameters are lower, and minima occur in S_{E2O1} while they are shifted in S_{O1E2}, due to dependence of interferences on length. Resulting O/E bandwidth is 350 GHz.

C. Two-Port Configurations

Fig. 5 shows the scattering parameters of the two-port configuration defined in Section V-C. As a matter of fact, it combines the two three-port configurations (36) and (37). The TWPD is again as in Section VI-A.1 (Fig. 2), except that both *electrical port $E1$ and optical port $O2$ are open and the length is reduced by a factor of ten* ($L_{\rm pin} = 50\ \mu$m). This length reduction is necessary to see the effect of the open-ended load because the optical power is almost totally converted over a 500-μm length before reaching the reflective load at $O2$. The

four relevant parameters are shown in magnitude only. The parameter relevant for the optical path is now the input reflection coefficient S_{O1O1} at port $O1$. It has a nonnegligible magnitude since a significant part of the optical beam reaches the reflective load at port $O2$, and travels back toward $O1$, while being partially absorbed. Since the optical power travels twice along the length, more power is absorbed and converted. As expected, the total power delivered to the output $E2$ [see Fig. 5(c)] is larger than in Fig. 2(c): it simultaneously takes advantage of the fact that reflected optical beam and photogenerated RF power travel twice in the device. The 3-dB bandwidth of S_{E2O1} is reduced (300 GHz) with respect to the corresponding four-port matched case $L_{\rm pin} = 50\ \mu$m (450 GHz). This is in accordance with the general property that reflections in a transmission line limit the frequency bandwidth of the line. The observed bandwidth is comparable, however, to that of the previous three-port configuration with $L_{\rm pin} = 50\,\mu$m (350 GHz). The present configuration has the advantage that the power delivered to output $E2$ is larger.

VII. Conclusion

In this paper, a complete distributed S-matrix characterization of mesa p-i-n TWPD's has been presented. It is valid for active as well as passive devices, reciprocal or not. Distributed equivalent circuits are first established. They take into account transmisssion-line parameters, modeling simultaneously the wanted detection and spurious emission of light inside of the device. Based on those circuits, a 4×4 scattering matrix formalism has been derived. It is used to predict the performances of the device. This scattering matrix formalism can be used to yield an efficient optimization tool; for instance, for maximizing the bandwidth of TWPD's, by varying the type of loads at each of the four ports of the device. This will be shown in a forthcoming paper, as well as other bandwidth limiting effects such as the finite carrier transit time and RF losses in the device.

Acknowledgment

The authors are grateful to Dr. M. Serres, Dr. Z. Zhu, Dr. R. Gillon, and Dr. B. Stockbroeckx for fruitful discussions.

References

[1] K. Giboney, J. Bowers, and M. Rodwell, "Travelling-wave photodetectors," in *IEEE MTT-S Int. Microwave Symp. Dig.*, 1995, pp. 159–162.

[2] D. Jäger, R. Kremer, and A. Stohr, "Travelling-wave optoelectronic devices for microwave applications," in *IEEE MTT-S Int. Microwave Symp. Dig.*, 1995, pp. 163–166.

[3] K. Giboney, R. Nagarajan, T. Reynolds, S. Allen, R. Mirin, and M. Rodwell, "Travelling-wave photodetectors with 172-GHz bandwidth and 76-GHz bandwidth-efficiency product," *IEEE Photon. Technol. Lett.*, vol. 7, pp. 412–414, Apr. 1995.

[4] K. S. Giboney, M. J. W. Rodwell, and J. E. Bowers, "Traveling-wave photodetector theory," *IEEE Trans. Microwave Theory Tech.*, vol. 45, pp. 1310–1319, Aug. 1997.

[5] B. S. Verma, R. Bhattacharyya, and V. V. Shah, "Optical admittance of an all-dielectric unsymmetrical multilayer near the monitoring wavelength," *Appl. Opt.*, vol. 25, no. 2, p. 315, Jan. 1986.

[6] R. T. Hawkins, II, M. D. Jones, S. H. Pepper, J. H. Goll, and M. K. Ravel, "Vector characterization of photodetectors, photoreceivers, and optical pulse sources by time-domain pulse response measurements," *IEEE Trans. Instrum. Meas.*, vol. 41, p. 467, Aug. 1992.

[7] H. Vifian, "Optical measurements based on RF modulation techniques," *IEEE Trans. Instrum. Meas.*, vol. 39, p. 982, Dec. 1990.

[8] D. D. Curtis and E. E. Ames, "Optical test set for microwave fiber-optic network analysis," *IEEE Trans. Microwave Theory Tech.*, vol. 38, p. 552, May 1990.

[9] B. Stockbroeckx, P. Dellisse, and A. Vander Vorst, "S-matrix definition for microwave optical transducers," *Microwave Opt. Technol. Lett.*, vol. 7, no. 17, pp. 2099–2106, Dec. 1994.

[10] A. Vander Vorst and D. Vanhoenacker, *Bases de l'Ingénierie Microonde*. Brussels, Belgium: De Boeck-Université, 1996.

[11] V. M. Hielata, G. A. Vawter, T. M. Brennan, and B. E. Hammons, "Traveling-wave photodetectors for high-power, large-bandwidth applications," *IEEE Trans. Microwave Theory Tech.*, vol. 43, pp. 2291–2298, Sept. 1995.

[12] Z. Zhu, R. Gillon, and A. Vander Vorst, "A new approach to broadband matching for pin photodiodes," *Microwave Opt. Technol. Lett.*, vol. 8, no. 1, pp. 8–13, Jan. 1995.

[13] I. Huynen, A. Salamone, and M. Serres, "A traveling wave model for optimizing the bandwidth of p-i-n photodetectors in silicon-on-insulator technology," *IEEE J. Select. Topics Quantum Electron.*, vol. 4, pp. 953–963, Nov.–Dec. 1998.

[14] Z. Zhu, I. Huynen, and A. Vander Vorst, "An efficient microwave characterization of PIN photodiodes," in *Proc. 26th European Microwave Conf.*, vol. 2, Prague, Czech Republic, Sept. 1996, pp. 1010–1014.

[15] J. Katz, S. Margalit, C. Harder, D. Wilt, and A. Yariv, "The intrinsic electrical equivalent circuit of a laser diode," *IEEE J. Quantum Electron.*, vol. QE-17, pp. 4–7, Jan. 1981.

Isabelle Huynen (S'87–M'89) was born in Belgium, in 1965. She received the electrical engineer degree and the Ph.D. degree in applied sciences from the Université Catholique de Louvain (UCL), Louvain-la-Neuve, Belgium, in 1989 and 1994, respectively.

In 1989, she joined the Microwave Laboratory, UCL, where she is currently a Research Associate of the National Fund for Scientific Research, Belgium. Her main research deals with electromagnetic (EM) theory using variational principles and measurement techniques applied to microwave, millimeter-wave, and optical circuits, with particular interest devoted to gyrotropic and nanoscale devices and materials in view of synthesizing hybrid and integrated circuits for telecommunications applications.

Dr. Huynen is member of the Belgian Society of Telecommunication and Electronic Engineers (SITEL) and the Royal Society of Belgian Electricians (SRBE/KVBE).

André Vander Vorst (M'64–SM'68–F'86) was born in Brussels, Belgium, in 1935. He received the electrical and mechanical engineer degrees and the Ph.D. degree in applied sciences from the Université Catholique de Louvain, Louvain-la-Neuve, Belgium, in 1958 and 1965, respectively, and the M.Sc. degree in electrical engineering from the Massachusetts Institute of Technology (MIT), Cambridge, in 1965.

He then joined Stanford University. He then founded the Microwaves Laboratory, UCL, which he currently heads. He has been involved in all the research activities of the Laboratory, beginning with loaded waveguides and cavities, then with atmospheric transmission and diffraction up to 300 GHz, designing and measuring active and passive circuits up to and above 100 GHz, and microwave bioelectromagnetics. His current interests are with microwave-optical transducers, humanitarian demining, and the interaction of EM fields with the nervous system. He has authored or co-authored three textbooks, several book chapters, and a variety of scientific and technical papers published in international journals and proceedings.

Dr. Vander Vorst is a member of the National Committee of URSI, Academia Europaea, The Electromagnetics Academy, and of various committees on communications, microwaves, and education. He has been active in IEEE Region 8, as well as in the European Microwave Conferences. He received the 1986 Sitel Prize, and the 1994 Meritorious Service Award presented by the IEEE Microwave Theory and Techniques Society (IEEE MTT-S).